Current Biology, Volume *30*

Supplemental Information

The Cellular and Mechanical Basis for Response Characteristics of Identified Primary Afferents in the Rat Vibrissal System

Takahiro Furuta, Nicholas E. Bush, Anne En-Tzu Yang, Satomi Ebara, Naoyuki Miyazaki, Kazuyoshi Murata, Daichi Hirai, Ken-ichi Shibata, and Mitra J.Z. Hartmann

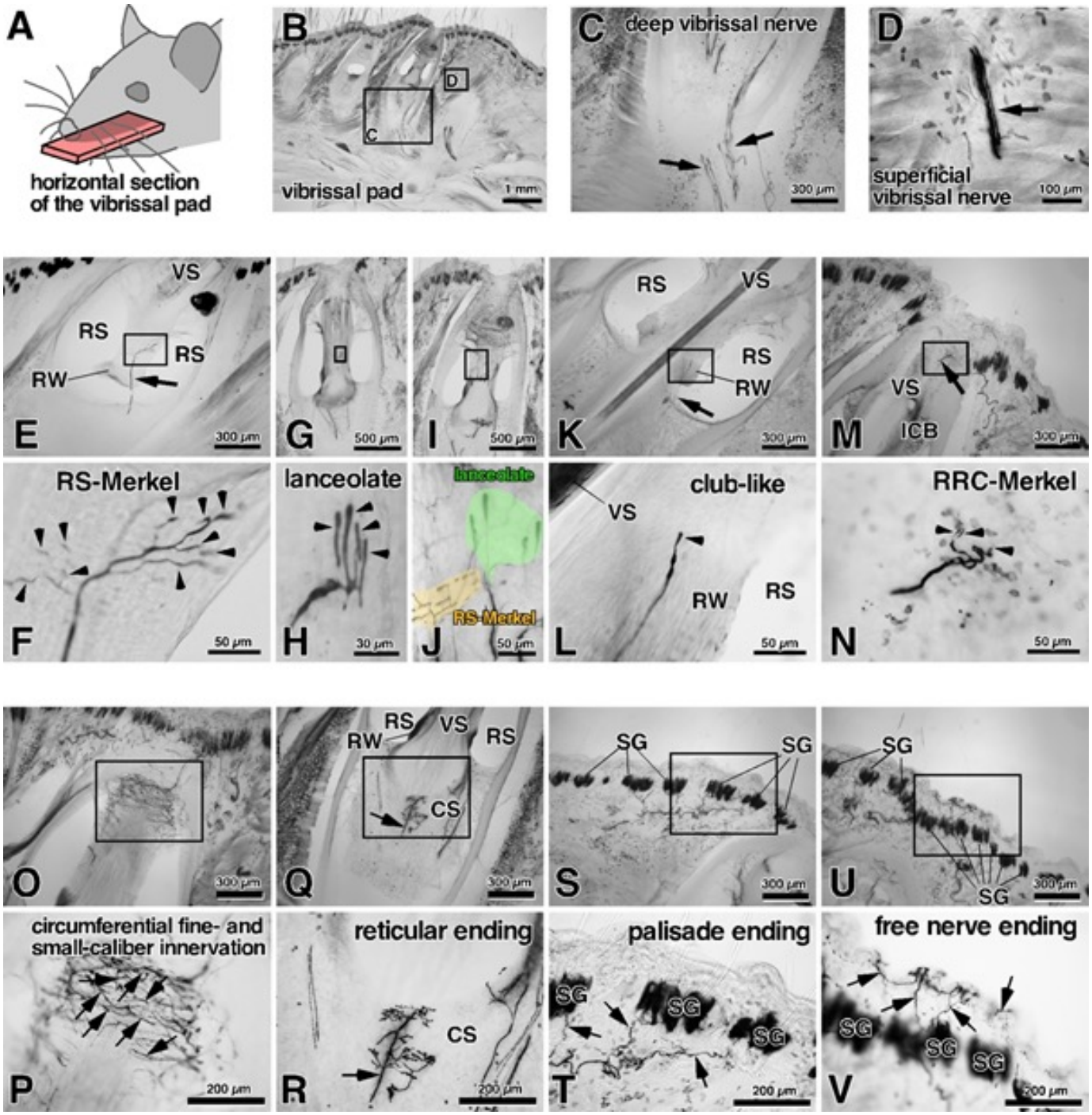

Figure S1. Bulk tracer injections reveal mechanoreceptor morphology and location within the follicle. Related to Figure 1. (A) All sections were made parallel to the horizontal plane. **(B)** The main bundle of the infraorbital nerve divides into many small bundles under the vibrissal pad. **(C)** Deep vibrissal nerves enter into the follicles at the level of the cavernous sinus, indicated by arrows. **(D)** A second nerve bundle, which runs toward the surface of the skin, contains the superficial vibrissal nerve. **(E-N)** The deep vibrissal nerve gives rise to several types of nerve endings in the follicle: Merkel endings at the ring sinus level (RS-Merkel), lanceolate endings, and club-like endings. The superficial vibrissal nerve provides Merkel endings at the rete ridge collar (RRC-Merkel). In each subplot, the bottom figure shows the expanded view in the region indicated by the rectangle in the top figure. **(O, P)** The superficial vibrissal nerve innervates circumferential fine- and small-caliber fibers. **(Q, R)** The deep vibrissal nerve innervates reticular endings. The infraorbital nerve also branches to innervate the skin through palisade endings **(S, T)**, and free nerve endings **(U, V)**. Arrows indicate visualized axons. Abbreviations: CS: cavernous sinus; ICB: inner conical body; OCB: outer conical body; RS: ring sinus; RW: ringwulst; SG: sebaceous gland; VS: vibrissal shaft.

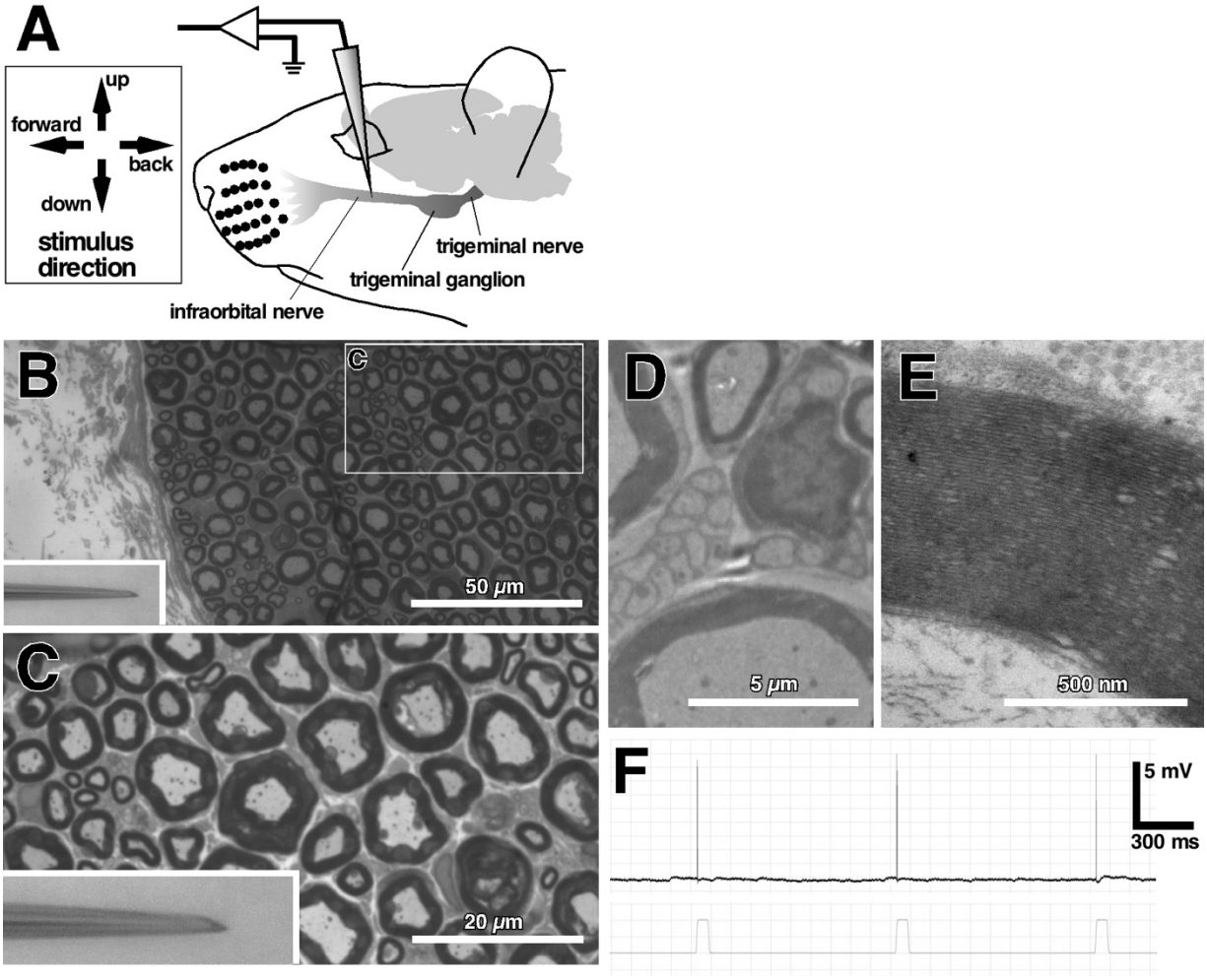

Figure S2. Recording setup and comparison of the size of the glass recording electrode with the size of axons in the infraorbital nerve. Related to Figures 1, 2, and 3. (A) The location of the intra-axonal recordings. **(B)** A transverse section shows the surface of the infraorbital nerve from which the sheath of dura was removed. Rectangle shows the region expanded in **(C)**. Insets in the bottom left of both (B) and (C) show the glass electrode used in the present study. **(D)** Electron microscopic photographs show that the infraorbital nerve contains myelinated axons of various thickness as well as unmyelinated axons. **(E)** Thick axons were coated by a thick myelin sheath. **(F)** An example of an intra-axonal recording.

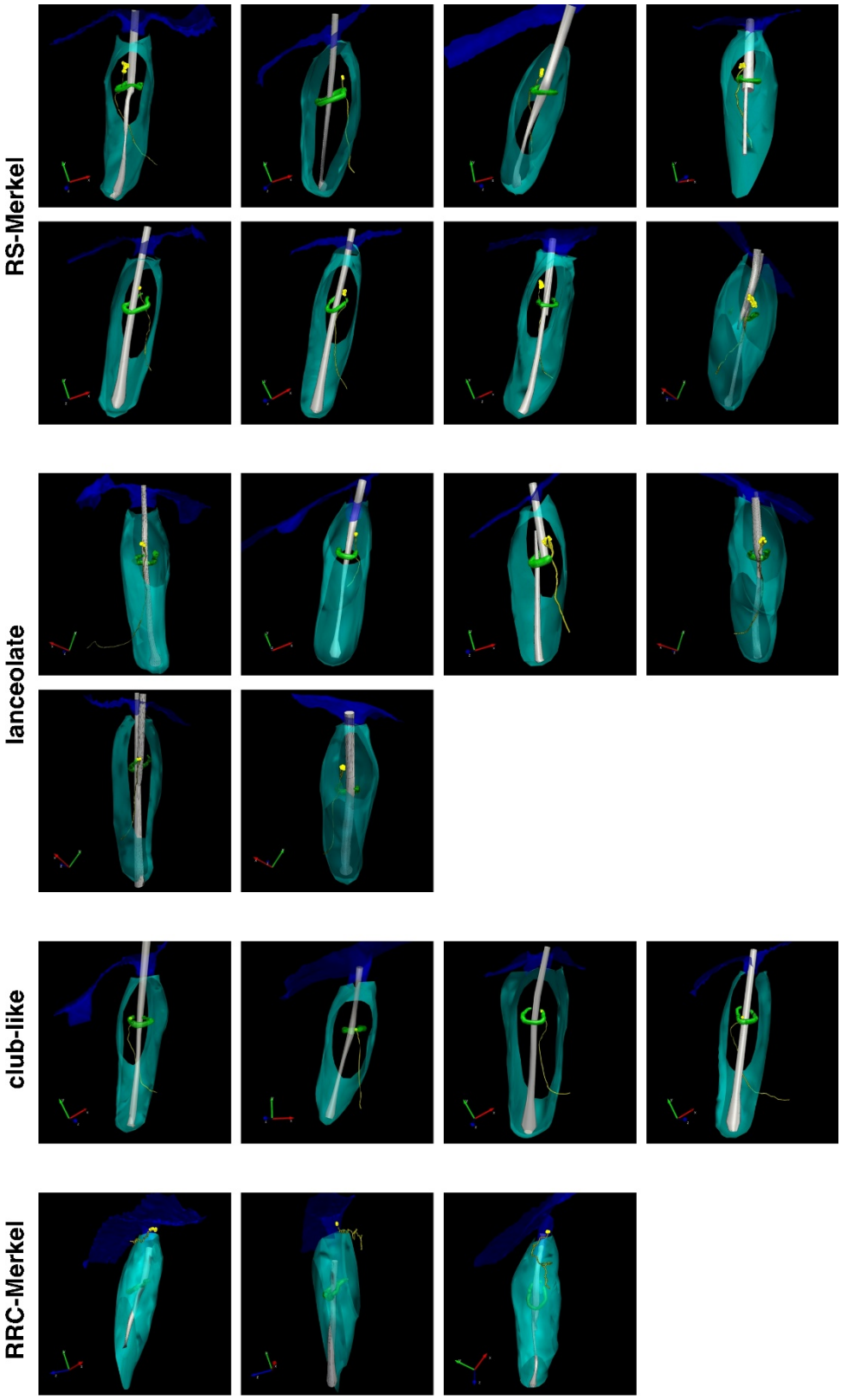

Figure S3. Three dimensional reconstruction of the follicles containing the recorded axons. Related to Figures 1 and 3. The first two rows show Merkel endings at the level of the ring sinus (RS-Merkel). The third and fourth rows show lanceolate endings. The fifth and sixth rows show club-like endings and Merkel endings at the rete ridge collar (RRC-Merkel), respectively. Axons and terminals are yellow while the skin, follicle capsule, vibrissal shaft, and ringwulst are shown in blue, cyan, gray and green, respectively. Thickness of axons and size of terminals in this figure are exaggerated for visual clarity. Red, green and blue arrows respectively indicate caudal, lateral and ventral directions.

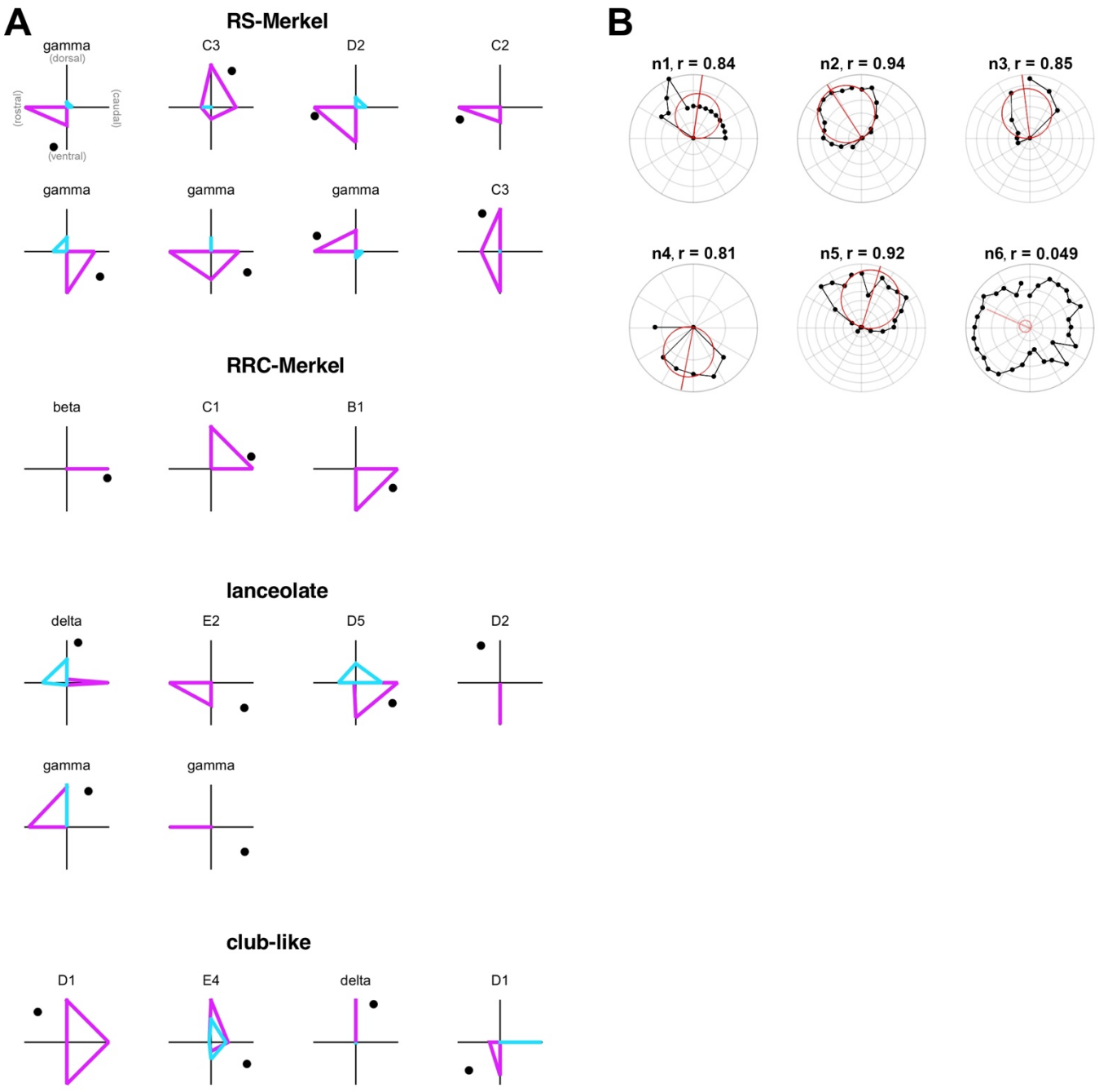

Figure S4. Angular tuning of different afferent types. Related to Figure 4. (A) Angular tuning curves for the 21 primary afferents recorded in the present study are shown as "radar plots." The four directions of whisker displacement (rostral, ventral, caudal, and dorsal) are indicated in the schematic in the top left. In each subplot the black filled circle indicates the position of the nerve endings. Pink polar plots indicate the magnitude of the ON response, and cyan polar plots indicate the magnitude of the OFF response. In each subplot responses have been normalized by the magnitude of the maximum response for that axon**. (B)** "Radar plots" of the ON responses of six unidentified, slowly-adapting afferents. Responses were recorded as the whisker was deflected in either 16 or 32 directions. Cosine fits appear as red circles, and are shown for five of the six afferents. The red line going through each circle indicates the afferent's "preferred direction" as computed from the cosine fit (eq. 4 in *Methods*). Based on their firing characteristics five of the six afferents (n1 – n5) are thought to be RS-Merkel. The sixth afferent (n6) responded strongly in all directions, and was therefore thought not to be an RS-Merkel ending. The title of each subplot indicates neuron number (e.g., n1) and the Pearson correlation (r) value computed between the experimental data and the cosine fit.

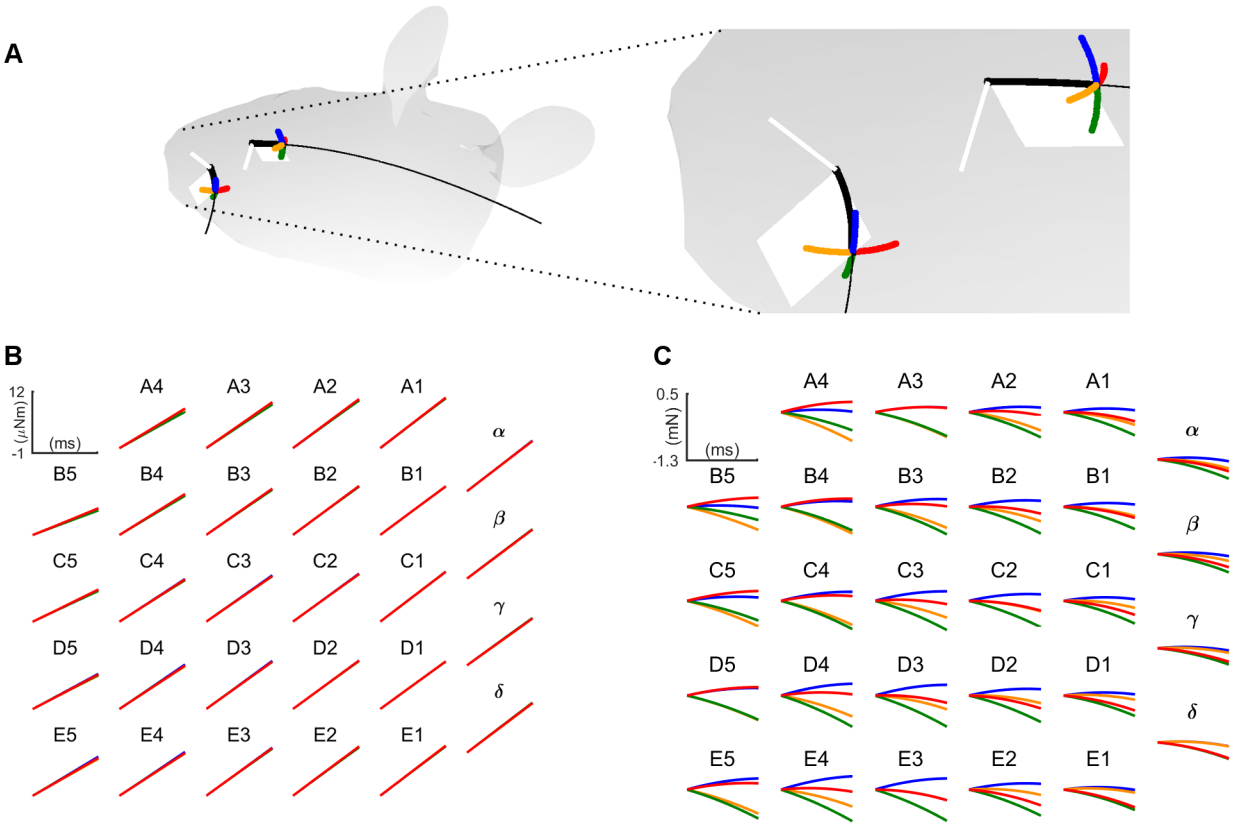

Figure S5. Three-dimensional vibrissal geometry strongly influences the axial force generated at the whisker base. Related to Figure 5. In all panels red represents caudal, yellow is rostral, blue is dorsal and green is ventral. **(A)** The D5 and gamma vibrissae are illustrated with the rat's head placed to align bregma with lambda, as in experiments. Thin and thick black lines indicate vibrissal shape before and after trimming to 5 mm. Although piezo stimulation displaces the vibrissa in head-centered coordinates, the mechanical effect of these displacements must be computed in vibrissa-centered coordinates. Vibrissa-centered coordinates depend on the geometry of each individual vibrissa, with the origin placed at the vibrissa base. For each whisker, the x-y plane is defined as the plane of its intrinsic curvature; this is the plane in which the proximal ~60% of the vibrissa lies. The two white trapezoids indicate the x-y planes that contain the two vibrissae. The x-axis is parallel to the vibrissa's length near its base, with positive pointing away from the vibrissa base. The y-axis is perpendicular to the x-axis, with positive pointing towards the vibrissa tip. Solid white lines represent the z-axes normal to these planes. The D5 and gamma emerge from the face at very different 3D angles and have different intrinsic curvatures. These different geometries will strongly affect the mechanical responses generated by deflection in the four directions indicated. For visual clarity, all four deflections are exaggerated to 25° instead of 5°. **(B)** Bending moment M_B shows similar responses across all vibrissae in all deflection directions. Only the response during the ON ramp is shown. **(C)** Each vibrissa exhibits a very different axial force, F_X, to the identical stimulation. Only the response during the ON ramp is shown. The axial force is the force directed "longitudinally," along the length of the vibrissa, parallel to its base.

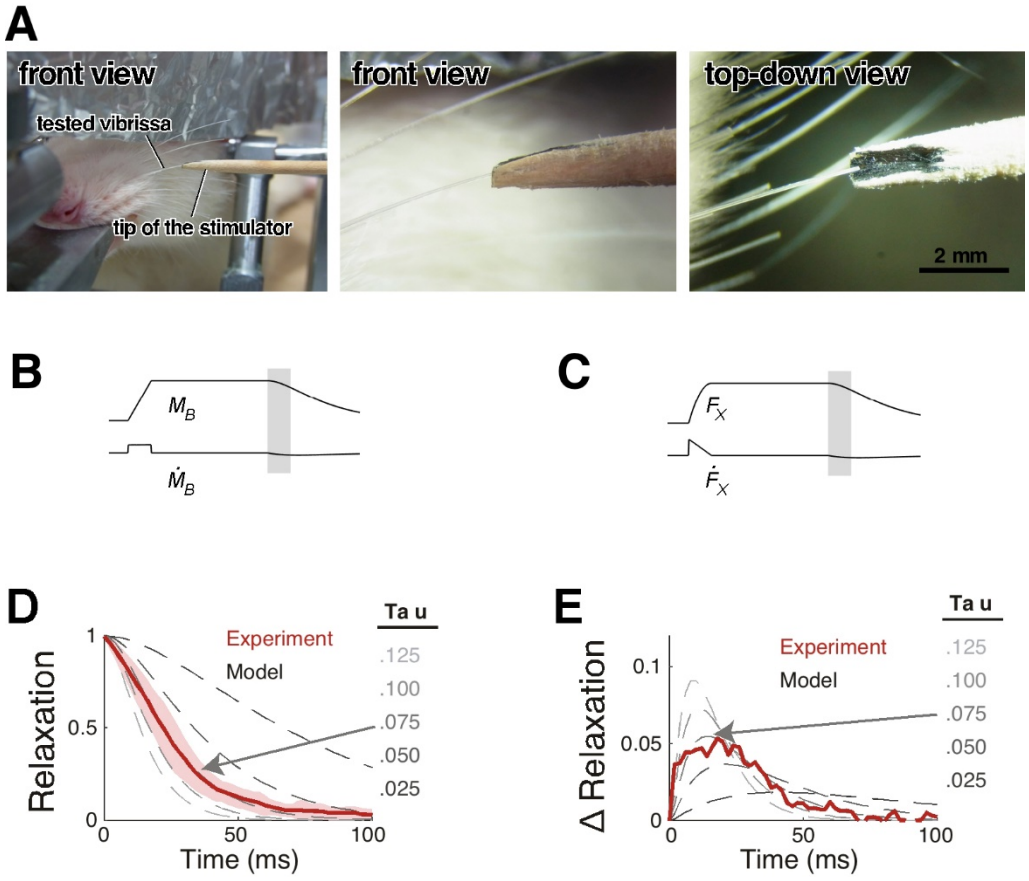

Figure S6. Attachment of the piezo stimulator to the tested vibrissa, and experimental determination of the tissue relaxation time constant. Related to Figure 5 and STAR*Methods. (A) The vibrissa was cut 5 mm from the skin, and the tip of the vibrissa was then inserted into the groove of a beveled straw attached to a ceramic bimorph bender. **(B,C)** Schematic of mechanical signals for a single deflection. Mechanics during the onset ramp is governed by piezoelectric deflection, while that during the offset ramp (shaded gray) is governed by tissue relaxation. **(B)** Schematics of M_B and its derivative. **(C)** Schematics of F_X and its time derivative. **(D)** Mean normalized angular position aligned to the time of release (0ms) for 44 whisker deflections of whisker D2 (red). Relaxation of 1 indicates fully deflected, 0 indicates rest position. Shaded region is +/- 1 S.D. Grayscale dashed lines show the relaxation function used in biomechanical models for several values of the τ parameter. **(E)** The temporal derivative of data and models shown in (D). Red line is the discrete difference of the mean experimental relaxation curve in (D). Grey dashed lines indicate temporal derivatives of the relaxation function for several values of τ. Data in E are inverted about the x-axis for visualization.

Cell number	Morphological type	Whisker identity	Latency in best direction (ms)	Magnitude in best direction (spikes/10 ms)	D-index	Terminal position (degrees)
1	RS Merkel	gamma	2.35	6.9	0.76	252
2	RS Merkel	C3	1.25	4.45	0.38	60
3	RS Merkel	D2	2.35	4.4	0.71	192
4	RS Merkel	C2	2.25	2.85	0.78	197
5	RS Merkel	gamma	2.65	3	0.72	323
6	RS Merkel	gamma	2.25	3	0.32	330
7	RS Merkel	gamma	2.35	6	0.75	158
8	RS Merkel	C3	3.35	2	0.19	115
9	lanceolate	delta	2.05	1.8	0.88	74
10	lanceolate	E2	3.45	2.4	0.74	323
11	lanceolate	D5	4.45	1.2	0.68	331
12	lanceolate	D2	5.85	1	1	117
13	lanceolate	gamma	2.45	1.05	0.71	59
14	lanceolate	gamma	6.05	1	1	324
15	club-like	D1	3.05	2	0.33	134
16	club-like	E4	1.25	4.55	0.52	329
17	club-like	delta	5.05	0.95	1	65
18	club-like	D1	4.15	0.8	0.8	222
19	RCC Merkel	beta	7.95	1	1	347
20	RCC Merkel	C1	6.75	1	0.71	17
21	RCC Merkel	B1	5.55	1	0.71	333

Table S1. Characteristics of the 21 primary afferents recorded in the present study. Related to Figure 1. *Latency* is defined as the duration to the occurrence of the first spike when the whisker is deflected in its best direction. *Magnitude* is defined as the average number of spikes in onset window of 10 ms when the whisker is deflected in its best direction. *Direction index* (D-index) is defined as the magnitude of the vector sum of the responses in all four stimulus directions normalized by the total number of spikes in all directions. The D-index ranges from 0, when the responses are equal in all stimulus directions, to 1, when a response is obtained only for a single stimulus direction. *Terminal position* is measured in degrees, with 0° representing caudal and 90º representing dorsal.